Numerical Studies of Critical Points of the Long-range Transverse-field Ising Chain

Xinyang Shen

Master's thesis
2026:E90



Lund University

Faculty of Science
Centre for Mathematical Sciences
Computational Science

Centrum Scientiarum Mathematicarum

Numerical studies of critical points of the long-range transverse-field Ising chain

Xinyang Shen

Thesis supervisor: Hong-Hao Tu, Anders Irbäck

Date: July 2, 2026

Abstract

The criticality of the ferromagnetic long-range transverse-field Ising chain (LRTFIC) with periodic boundary conditions and power-law decaying Ising coupling is studied using the Density Matrix Renormalization Group (DMRG). The ground states of the systems at different values of the transverse field h are obtained using DMRG. From these ground states, a quantity called crosscap overlap can be extracted efficiently. This thesis suggests that the crosscap overlap can serve as an indicator to identify the critical points of the LRTFIC. The estimated critical points are further verified by data collapse. For the decay exponent $\alpha = 3.5$, the LRTFIC belongs to the short-range regime. DMRG is performed on systems with different sizes up to $N = 280$. The critical point is estimated to be $h_c \approx 1.25$, at which the crosscap overlaps approach the exact value of the short-range Ising chain as the system size grows.

Popular scientific summary

Fasövergångar beskriver hur materia kan ändra sitt tillstånd. Till exempel fryser vatten till is eller kokar till ånga när temperaturen ändras. Temperaturen vid vilken en fasövergång sker är den kritiska punkten. Runt den kritiska punkten uppvisas många intressanta beteenden. I vissa kvantmaterial kan dock en tillståndsförändring ske även vid absoluta nollpunkten, där vanlig termisk rörelse har försvunnit. Dessa förändringar kallas kvantfasövergångar. De drivs av kvanteffekter och av externa parametrar såsom magnetfält.

Denna avhandling studerar en enkel men viktig modell: Isingkedjan med långräckviddig transversellt fält. Man kan föreställa sig den som en linje av många magneter. Varje magnet tenderar att rikta in sig med de andra, medan ett externt fält försöker vrida dem i en annan riktning. När fältet är svagt föredrar magneterna att peka tillsammans. När fältet är starkt dominerar det externa fältet. Mellan dessa två faser finns det en kritisk punkt, där systemet ändras från en typ av beteende till en annan. Det särskilda med modellen som studeras här är att magneterna inte bara interagerar med sina närmaste grannar. De kan också känna magneter längre bort, men denna påverkan blir svagare med avståndet. Sådana långräckviddiga interaktioner är relevanta för moderna kvantsimulatorer, till exempel system gjorda av fångade joner eller högt exciterade atomer, där interaktionernas styrka och räckvidd kan kontrolleras experimentellt.

Avhandlingens huvuduppgift är att lokalisera den kritiska punkten för den långräckviddiga modellen med hjälp av numeriska simuleringar. Metoden, densitetsmatrisrenormaliseringsgruppen, är ett kraftfullt sätt att approximera det lägsta energitillståndet hos ett stort kvantsystem. Från detta tillstånd extraherar avhandlingen en storhet som kallas crosscap overlap, vilken används som en indikator för att lokalisera de kritiska punkterna. Resultaten visar att crosscap overlap kan användas för att identifiera den kritiska punkten för den långräckviddiga Isingkedjan inom det studerade parameterområdet.

Acknowledgements

I am deeply grateful to my supervisor Hong-Hao for the detailed guidance throughout this project. His careful suggestions on scientific writing greatly improved the structure and readability of this thesis. I would also like to thank Wei Tang for providing valuable programming help in Julia, which made the implementation and debugging stages of the numerical work more efficient. Additionally, I am sincerely thankful to my co-supervisor Anders for helping me access the necessary computational resources. Finally, I acknowledge the use of ChatGPT for checking the typos and grammar of the written text, as well as OpenCode for the improvement of code.

List of abbreviations

1D	One-Dimensional
2D	Two-Dimensional
CFT	Conformal Field Theory
DMRG	Density Matrix Renormalization Group
FSS	Finite-Size Scaling
LRTFIC	Long-Range Transverse-Field Ising Chain
LRTFIM	Long-Range Transverse-Field Ising Model
MPO	Matrix Product Operator
MPS	Matrix Product State
OBC	Open Boundary Condition
PBC	Periodic Boundary Condition
QPT	Quantum Phase Transition
SVD	Singular Value Decomposition
TFIC	Transverse-Field Ising Chain
TFIM	Transverse-Field Ising Model

Contents

1 Introduction **13**

2 Density Matrix Renormalization Group (DMRG) **15**
2.1 Tensor networks 15
2.1.1 Matrix Product States (MPS) 16
2.1.2 Matrix Product Operators (MPO) 20
2.2 DMRG algorithm 21

3 Quantum phase transitions **25**
3.1 Critical exponents 25
3.2 Quantum-classical mapping 26
3.3 Finite-size scaling 27
3.4 Crosscap overlaps 28

4 Some exactly solvable models and their DMRG results **31**
4.1 The Heisenberg chain 31
4.2 The XXZ chain 31
4.3 The Haldane-Shastry model 33
4.4 The transverse-field Ising chain 33

5 The long-range transverse-field Ising chain (LRTFIC) **35**
5.1 Previous studies on the LRTFIC 35
5.1.1 Limiting cases of the LRTFIC 35
5.1.2 Critical regimes of the LRTFIC 36
5.2 DMRG results on the LRTFIC 37

6 Summary and outlook **41**

Chapter 1

Introduction

Quantum phase transitions (QPTs) are one of the essential subjects in condensed matter physics and quantum many-body problems. QPTs occur at zero temperature, at which the thermal fluctuations are eliminated and the quantum fluctuations take effect, and are governed by a non-thermal parameter such as pressure or an external field. The transverse-field Ising model (TFIM) has long been one of the paradigmatic models for studying QPTs. The 1D TFIM, transverse-field Ising chain (TFIC), which is exactly solvable and can be mapped to the 2D classical Ising model, has been comprehensively studied both theoretically [1, 2] and experimentally [3, 4].

The TFIM only contains nearest-neighbor interactions. However, many quantum simulators like Rydberg gas [5], trapped ions [6], and real-world materials like spin ice [7] and the dipolar interaction material $LiHoF_4$ [8] have long-range interactions. This thesis focuses on the ferromagnetic long-range transverse-field Ising chain (LRTFIC), whose Hamiltonian is

$$H = -\sum_{1\le i<j\le N} J_{ij}\sigma_i^z\sigma_j^z - h\sum_{i=1}^{N}\sigma_i^x,$$

where h is the external field and the coupling strength J_{ij} follows a power-law decay with the decay exponent α, i.e., $J_{ij} \sim \frac{1}{|i-j|^\alpha}$. The LRTFIC is not exactly solvable, and the main theoretical methods to study it are mean-field theory and renormalization group [9–11]. Experimentally, quantum simulators with an adjustable decay exponent α can be realized by trapped ions [12]. Numerically, quantum Monte Carlo [13–16] and tensor networks [17–19] are the main methods to study its critical behaviors (such as locating critical points and computing critical exponents), by means of Binder cumulants and data collapse of magnetization and/or susceptibility. Both theoretical and numerical results support that there are three regimes of the LRTFIC, depending on the decay exponent α [9, 11, 16]. For $\alpha < 5/3$, the LRTFIC belongs to the long-range mean-field regime. For $\alpha > 11/4$, the LRTFIC belongs to the short-range regime. In between, the critical exponents vary continuously and connect the two regimes.

Very recently, the crosscap overlap has been proposed as an efficient way to study the critical behaviors of models that can be described by conformal field theory[1]. The crosscap

[1] At criticality, the systems have scale invariance. In many cases, the scale invariance can be promoted to conformal invariance, meaning the system is invariant under conformal transformations. Conformal field theory is a quantum field theory that studies such systems.

overlap is the overlap between a quantum state and a crosscap state[2]. Many quantities, such as the Klein bottle entropy [20] and Luttinger parameter [21], can be computed by crosscap overlaps. For the TFIC, the crosscap states are related to the Kramers-Wannier duality, and the universal scaling function associated with the perturbed TFIC can be obtained from the crosscap overlaps [22].

This thesis uses density matrix renormalization group (DMRG) to obtain the ground-state wavefunction of the LRTFIC and extract the crosscap overlap as an indicator of critical points. DMRG is one of the most accurate numerical methods, especially for 1D lattice models, and can give the ground-state energy and the ground-state wavefunction in the matrix product state (MPS) form, from which many observables including the crosscap overlap can be extracted efficiently. The theoretical studies of the crosscap overlap in the TFIC showed that it has an exact value at the critical point and is free from any finite-size corrections [22]. Therefore, the crosscap overlap can potentially be a good indicator of the critical points for the LRTFIC when its critical behaviors are the same as the TFIC with short-range interactions. Our results show that the finite-size corrections are significant for the LRTFIC, but a precise critical point can be obtained by a simple extrapolation. The critical points are obtained for three values of α, all of which are consistent with previous studies.

The thesis is structured as follows. Chapter 2 briefly reviews the tensor network notation, matrix product state, matrix product operator (MPO), and the DMRG algorithm. Chapter 3 briefly introduces the quantum phase transition and some related important concepts. Chapter 4 tests the DMRG algorithm on some exactly solvable spin-1/2 models, including the Heisenberg chain, the XXZ chain, the Haldane-Shastry chain and the TFIC, and shows how to use the crosscap overlap as an indicator of critical points. Chapter 5 first introduces previous studies on the LRTFIC along with its important properties, then explains the process of pinpointing the critical points of the LRTFIC, and finally presents the DMRG results on the LRTFIC with the obtained critical points. Chapter 6 summarizes this thesis and discusses future directions.

[2] A crosscap refers to a circle with all pairs of antipodal points identified (glued together). A crosscap state corresponds to the crosscap boundary condition of the cylinder obtained from quantum-classical mapping.

Chapter 2

Density Matrix Renormalization Group (DMRG)

In this chapter, we briefly review the DMRG method. We start by introducing the graphic notation of tensor networks in Section 2.1, and then discuss the DMRG algorithm in Section 2.2.

2.1 Tensor networks

We start by introducing the graphic notation of tensor networks. Consider a single spin-1/2 particle in a superposition state

$$|\psi\rangle = \sum_{s=0,1} A_s |s\rangle .$$

The superposition coefficients A_s form a tensor A (in this case, "vector"). The Hermitian conjugate of $|\psi\rangle$ is

$$\langle\psi| = \sum_{s=0,1} A_s^* \langle s| .$$

In the same basis, an operator O can be written as

$$O = \sum_{s,s'} O_{ss'} |s\rangle \langle s'| ,$$

where the coefficients $O_{ss'}$ form a tensor O (in this case, "matrix"). They are depicted in Fig. 2.1.

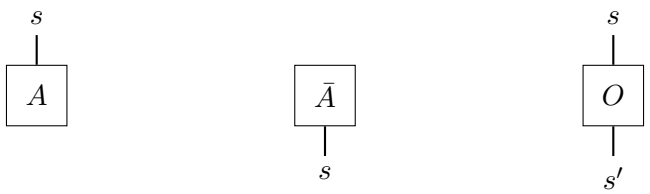


Figure 2.1: States and operators in the graphic notation.

Connecting two tensors means a summation over the index on the leg that is connected. By connecting these tensors, we can represent some physical quantities, such as the inner product

$$\langle\psi|\psi\rangle = \left(\sum_{s=0,1} A_s^* \langle s|\right)\left(\sum_{s=0,1} A_s |s\rangle\right) = \sum_{s=0,1} A_s^* A_s,$$

an operator acting on a state

$$O|\psi\rangle = \left(\sum_{s,s'} O_{ss'} |s\rangle \langle s'|\right)\left(\sum_{s=0,1} A_s |s\rangle\right) = \sum_s \left(\sum_{s'} O_{ss'} A_{s'}\right)|s\rangle,$$

and the expectation value of an operator

$$\langle\psi| O |\psi\rangle = \left(\sum_{s=0,1} A_s^* \langle s|\right)\left(\sum_{s,s'} O_{ss'} |s\rangle \langle s'|\right)\left(\sum_{s=0,1} A_s |s\rangle\right) = \sum_{s,s'} A_s^* O_{ss'} A_{s'}.$$

They are depicted in Fig. 2.2, respectively.

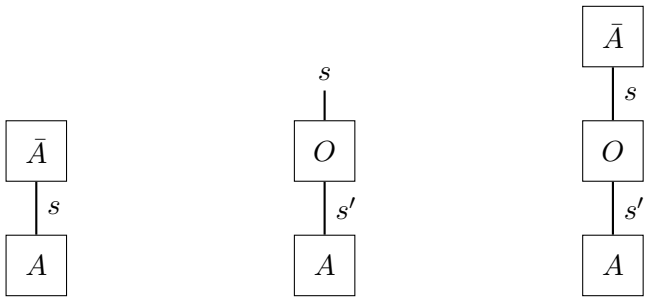


Figure 2.2: Some physical quantities in the graphic notation.

In summary, a free leg means a degree of freedom that is not summed over, and a connected leg means a summation over the index on that leg. After the summation, two or more tensors form a new tensor if there are free legs, or a scalar if all legs are connected. This is the so-called tensor contraction.

2.1.1 Matrix Product States (MPS)

Consider an N-site spin-1/2 chain. To represent the state

$$|\psi\rangle = \sum_{s_1,s_2,\cdots,s_N} A_{s_1 s_2 \cdots s_N} |s_1 s_2 \cdots s_N\rangle$$

we need a tensor A with 2^N elements, which becomes huge when N is large. To avoid this, we write the state in the matrix product form, known as a Matrix Product State (MPS) [23]:

$$|\psi\rangle = \sum_{s_1,s_2,\cdots,s_N} \left(\sum_{\alpha_1 \cdots \alpha_{N-1}} A^{[1]}_{s_1\alpha_1} A^{[2]}_{\alpha_1 s_2 \alpha_2} \cdots A^{[N-1]}_{\alpha_{N-2} s_{N-1} \alpha_{N-1}} A^{[N]}_{\alpha_{N-1} s_N}\right) |s_1 s_2 \cdots s_N\rangle.$$

Fig. 2.3 shows the graphic notation of an MPS. The bond index $\alpha_j = 1, 2, \cdots, D_j$ with $j = 1, 2, \cdots, N-1$, where D_j is the right bond dimension of the tensor $A^{[j]}$. If a fixed bond dimension D is used for all tensors, then only about $2ND^2$ parameters are needed to parametrize $|\psi\rangle$. We call D the bond dimension of the MPS. Note that the MPS itself does not avoid the exponential cost; the cost is reduced to polynomial after the bond dimension D is restricted to a fixed value.

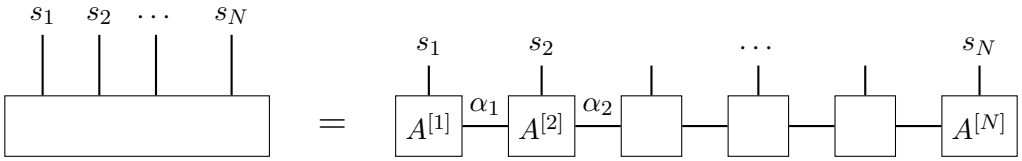


Figure 2.3: MPS in the graphic notation.

A state (of a finite system) can be written as an MPS exactly. Consider a system divided into two parts, $\mathcal{H}_\mathcal{A}$ and $\mathcal{H}_\mathcal{B}$; the state of the system can be written with the Schmidt decomposition

$$|\psi\rangle = \sum_{i=1}^{\chi} \sigma_i \left|\phi_i^A\right\rangle \left|\phi_i^B\right\rangle,$$

where $\left|\phi_i^A\right\rangle$ and $\left|\phi_i^B\right\rangle$ form orthonormal bases in Hilbert space $\mathcal{H}_\mathcal{A}$ and $\mathcal{H}_\mathcal{B}$, respectively. The Schmidt coefficients σ_i satisfy $\sigma_i > 0$ and $\sum_{i=1}^{\chi} \sigma_i^2 = 1$. The Schmidt rank χ gives the number of terms, and the square of Schmidt coefficient gives the weight of each term. Numerically, the Schmidt decomposition on a state is equivalent to the singular value decomposition (SVD) on the tensor. First, divide site 1 from the rest by performing SVD on $A_{s_1, s_2 \cdots s_N}$:

$$A_{s_1,(s_2\cdots s_N)} = \sum_{\alpha_1=1}^{\chi_1} U_{s_1,\alpha_1} \lambda_{\alpha_1} (V^\dagger)_{\alpha_1,(s_2\cdots s_N)}.$$

where α_1 is the bond index and $A^{[1]}_{s_1\alpha_1} = U_{s_1,\alpha_1}$ is the local tensor at site 1. Then continue performing SVD on $\lambda V^\dagger$, we can divide site 2 from the rest and get $A^{[2]}$. Continue the process we can convert the original tensor A to an MPS. Therefore, the bond dimension D_i of a local tensor in an MPS corresponds to the Schmidt rank across a bipartition. To justify a constant bond dimension can be used, we need the entanglement entropy.

The entanglement entropy is defined as

$$S = -\sum_{i=1}^{\chi} \sigma_i^2 \ln \sigma_i^2.$$

With the constraint $\sum_{i=1}^{\chi} \sigma_i^2 = 1$, S gets its maximum $\ln \chi$ when $\sigma_i^2 = \frac{1}{\chi}\ \forall i$. This means that, to represent the state with an MPS precisely, the bond dimension must satisfy

$$D > \chi \sim e^S.$$

For 1D gapped systems with local interactions, the entanglement of its ground state satisfies the entanglement area law [24], which means that the entanglement entropy is of the order of

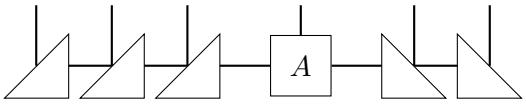


Figure 2.4: Mixed-canonical MPS. Tensors to the left of A are left-canonical, denoted by an isosceles triangle whose apex points to the bottom right. Tensors to the right of A are right-canonical, denoted by an isosceles triangle whose apex points to the bottom left. The mixed-canonical MPS is normalized if the tensor A itself is normalized.

the "area" of a 1D chain, i.e., $S \sim O(1)$ independent of system size. So an MPS with constant bond dimension D can be used to represent the state precisely. For 1D gapless systems that can be described by conformal field theory, there is a logarithmic violation of the area law [25]:

$$S(L) \sim \begin{cases} \frac{c}{6} \ln L & \text{open boundary condition (OBC)} \\ \frac{c}{3} \ln L & \text{periodic boundary condition (PBC),} \end{cases}$$

where c is the central charge[1]. This means that $D \sim e^S \sim L^{c/6}$ ($L^{c/3}$) is required. The increase of the bond dimension with system size is still mild.

In the DMRG algorithm, the canonical form of MPS is often required. A tensor in MPS is said to be left-canonical if the matrix A reshaped from the tensor $A^{[n]}$ by combining the left and physical indices is an isometry:

$$A^\dagger A = I, \quad \sum_{\alpha_{n-1}, s_n} (A^\dagger)_{\alpha'_n, (\alpha_{n-1} s_n)} A_{(\alpha_{n-1} s_n), \alpha_n} = \delta_{\alpha'_n \alpha_n},$$

where $\delta_{\alpha'_n \alpha_n}$ is the Kronecker symbol and $A_{(\alpha_{n-1} s_n), \alpha_n} = A^{[n]}_{\alpha_{n-1} s_n \alpha_n}$. It is said to be right-canonical if the matrix A reshaped from the tensor $A^{[n]}$ by combining the right and physical index is an isometry:

$$AA^\dagger = I, \quad \sum_{s_n, \alpha_n} A_{\alpha'_{n-1}, (s_n \alpha_n)} (A^\dagger)_{(s_n \alpha_n), \alpha_{n-1}} = \delta_{\alpha'_{n-1} \alpha_{n-1}},$$

where $A_{\alpha'_{n-1}, (s_n \alpha_n)} = A^{[n]}_{\alpha_{n-1} s_n \alpha_n}$. An MPS is said to be left(right)-canonical if all tensors are left(right)-canonical, and to be mixed-canonical if all tensors to the left of a tensor $A^{[n]}$ are left-canonical and all tensors to the right of this tensor are right-canonical. Fig. 2.4 shows the MPS in mixed-canonical form.

If the MPS is in a left-canonical form, contracting the $\langle \psi | \psi \rangle$ tensor network from left to right will always give the identity matrix. For example, first contract the tensors at site 1:

$$C_{\alpha'_1 \alpha_1} = \sum_{s_1} (A_{s_1 \alpha'_1})^* A_{s_1 \alpha_1} = \sum_{s_1} (A^\dagger)_{\alpha'_1 s_1} A_{s_1 \alpha_1} = \delta_{\alpha'_1 \alpha_1}.$$

Then continue to contract the tensors at site 2:

[1]The central charge c measures the effective number of degrees of freedom of a CFT. For example, $c = 1/2$ for Ising CFT.

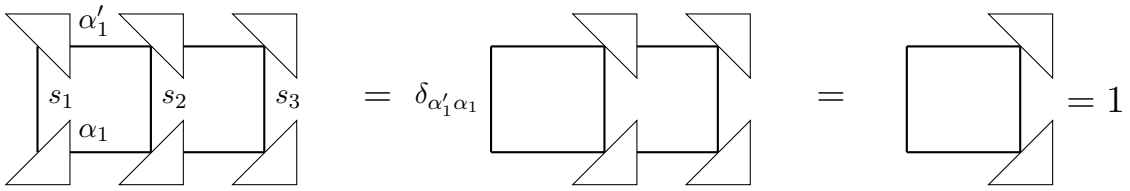


Figure 2.5: Contracting a left-canonical MPS from the left side.

$$C_{\alpha_2'\alpha_2} = \sum_{s_2,\alpha_1',\alpha_1} C_{\alpha_1'\alpha_1}(A_{\alpha_1' s_2 \alpha_2'})^* A_{\alpha_1 s_2 \alpha_2} = \sum_{s_2,\alpha_1',\alpha_1} \delta_{\alpha_1'\alpha_1}(A_{\alpha_1' s_2 \alpha_2'})^* A_{\alpha_1 s_2 \alpha_2}$$
$$= \sum_{\alpha_1,s_2} (A_{\alpha_1 s_2 \alpha_2'})^* A_{\alpha_1 s_2 \alpha_2} = \sum_{\alpha_1,s_2} (A^\dagger)_{\alpha_2',(\alpha_1 s_2)} A_{(\alpha_1 s_2),\alpha_2} = \delta_{\alpha_2'\alpha_2}.$$

Continuing to the last pair of tensors, we will get 1, which means that the MPS is normalized. Similarly, if the MPS is in a right-canonical form, then contracting the $\langle\psi|\psi\rangle$ tensor network from right to left will always give the identity matrix and the MPS is normalized. Fig. 2.5 shows the process of contracting a left-canonical MPS from the left side.

If the MPS is initially not in the canonical form, we can bring it into a canonical form. To do so, one can perform an SVD sweep or a QR sweep. Here we describe the SVD sweep, which canonicalizes the MPS site by site by moving the orthogonality center through the chain.

As an example, consider bringing an MPS into the right-canonical form. The sweep starts from the last site and moves from right to left. First, reshape the tensor $A^{[N]}$ into a matrix

$$A^{[N]}_{\alpha_{N-1},(s_N\alpha_N)} ,$$

where the left virtual index is kept as the row index and the physical index together with the right virtual index is combined into the column index. Performing an SVD gives

$$A^{[N]} = U\Sigma V^\dagger.$$

The matrix $V^\dagger$ satisfies $V^\dagger(V^\dagger)^\dagger = V^\dagger V = I$ and is therefore right-canonical. We replace the tensor at site N by $V^\dagger$, reshaped back into a three-index tensor. The remaining factor $U\Sigma$ is absorbed into the tensor on the neighboring site:

$$A^{[N-1]}_{\text{new}} = A^{[N-1]}U\Sigma.$$

After this step, the tensor $A^{[N]}_{\text{new}}$ is right-canonical, and the state $|\psi\rangle$ is unchanged. No approximation has been made if no singular values have been truncated. The same procedure is then applied to the updated tensor at site $N-1$: reshape it as a matrix, perform an SVD, keep the right-isometric factor as the new site tensor, and absorb the remaining factor into site $N-2$. Repeating this process until the first site is reached brings the whole MPS into right-canonical form.

A left-canonical form can be obtained analogously by sweeping from left to right. In that case, after reshaping the site tensor and performing an SVD, the left-canonical factor U is kept as the site tensor, while the factor $\Sigma V^\dagger$ is absorbed into the next tensor on the right. In both directions, the sweep changes only the gauge of the MPS and leaves the represented quantum state unchanged, unless an explicit truncation of singular values is introduced.

2.1.2 Matrix Product Operators (MPO)

A quantum state can be represented as an MPS, while a Hamiltonian can be represented as an MPO. Consider a simple Hamiltonian on an N-site chain:

$$H = \sum_{i=1}^{N} S_i.$$

It can be written as

$$\begin{aligned}\sum_{j=1}^{N} S_j^z &= \begin{pmatrix}0 & 1\end{pmatrix}\begin{pmatrix}I & 0\\ S_1^z & I\end{pmatrix}\begin{pmatrix}I & 0\\ S_2^z & I\end{pmatrix}\cdots\begin{pmatrix}I & 0\\ S_{N-1}^z & I\end{pmatrix}\begin{pmatrix}I & 0\\ S_N^z & I\end{pmatrix}\begin{pmatrix}1\\ 0\end{pmatrix}\\ &= \begin{pmatrix}S_1^z & I\end{pmatrix}\begin{pmatrix}I & 0\\ S_2^z & I\end{pmatrix}\cdots\begin{pmatrix}I & 0\\ S_{N-1}^z & I\end{pmatrix}\cdots\begin{pmatrix}I\\ S_N^z\end{pmatrix},\end{aligned}$$

where the matrix index corresponds to the virtual bond degrees of freedom. Fig. 2.6 shows the graphic notation of an MPO.

For Hamiltonians that are complicated, we need a finite-state machine to generate the MPO form [26]. Consider the transverse-field Ising chain with open boundary conditions. The Hamiltonian is

$$H = -\sum_{i=1}^{N-1}\sigma_i^z\sigma_{i+1}^z - h\sum_{i=1}^{N}\sigma_i^x.$$

First, we need to define the states:

- q_0: initial state, waiting for $-\sigma^z$ or $-h\sigma^x$;
- q_z: has received $-\sigma^z$, waiting for another σ^z at the next site;
- q_f: final state.

Second, we need to formulate the transfer rules, which specify what a valid state transfer is:

- q_0: can stay in q_0 by receiving I, or enter q_z by receiving $-\sigma^z$, or q_f by receiving $-h\sigma^x$;
- q_z: can enter q_f by receiving σ^z;
- q_f: can stay in q_f by receiving I.

Now we can construct the transfer table:

	q_0	q_z	q_f
q_0	I	$-\sigma^z$	$-h\sigma^x$
q_z			σ^z
q_f			I

where the empty entries are zeros, meaning invalid transfers. By multiplying the transfer tables, the MPO is obtained. The MPO for $N = 3$ is given as an example:

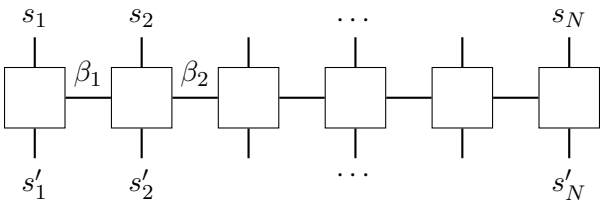


Figure 2.6: Graphic notation of MPO. β_1: row index of the transfer table; β_2: column index of the transfer table. When β_1 and β_2 are specified, it yields a matrix, with physical indices s_2 and s'_2.

$$\begin{bmatrix} I & -\sigma_1^z & -h\sigma_1^x \end{bmatrix} \begin{bmatrix} I & -\sigma_2^z & -h\sigma_2^x \\ 0 & 0 & \sigma_2^z \\ 0 & 0 & I \end{bmatrix} \begin{bmatrix} -h\sigma_3^x \\ \sigma_3^z \\ I \end{bmatrix}.$$

2.2 DMRG algorithm

With MPS and MPO constructed, we can use the DMRG algorithm to obtain the ground state and ground-state energy of a Hamiltonian. Furthermore, some observables can be extracted from the ground-state MPS.

For a given Hamiltonian H, we want to find a state $|\psi\rangle$ that minimizes $\langle\psi| H |\psi\rangle$ under the condition $|\psi\rangle$ is normalized. The DMRG algorithm achieves this by finding the optimal MPS as the variational solution to a Hamiltonian. In detail, the MPS with a fixed bond dimension form a variational class, and DMRG finds the best approximation to the ground state within this variational class, by minimizing the energy. As a variational method, the DMRG algorithm updates MPS site by site. To update site i, let A be the tensor at site i in MPS, and $|\psi(A)\rangle$ be the MPS in which site tensor A is a variable and the tensors at all other sites are fixed. We need to find the site tensor A which minimizes $\langle\psi(A)| H |\psi(A)\rangle$ and keeps $|\psi(A)\rangle$ normalized. It can be written as an optimization problem with a Lagrange multiplier,

$$E[A, \bar{A}, \lambda] = \langle\psi(A)| H |\psi(A)\rangle - \lambda(\langle\psi(A)|\psi(A)\rangle - 1), \tag{2.2.1}$$

where $\bar{A}$ is the complex conjugate of A. The graphic notation of Eq. (2.2.1) is shown in Fig. 2.7. First, we need to bring the MPS into a mixed-canonical form, which keeps $|\psi(A)\rangle$ normalized. Then, differentiating E with respect to $\bar{A}$, we get the tensor network shown in Fig. 2.8.

In the tensor network representation of $\langle\psi(A)| H |\psi(A)\rangle$, contracting the MPS and MPO tensors to the left of A, we get the left environment tensor C_L, and similarly the right environment tensor C_R. The C_L, C_R, together with the MPO tensor at this site, form an effective Hamiltonian tensor H_{eff}. Reshaping H_{eff} to matrix $(H_{\text{eff}})_{(\alpha_i\beta_i s_i),(\alpha'_i\beta'_i s'_i)}$ and the tensor A to a vector, it becomes a standard eigenvalue problem

$$H_{\text{eff}} A = \lambda A, \tag{2.2.2}$$

which is shown in Fig. 2.9. Solving this, we get the minimum eigenvalue $\lambda_{\min}$ and the corresponding eigenvector A_{new} as the variational ground-state energy and the update to A.

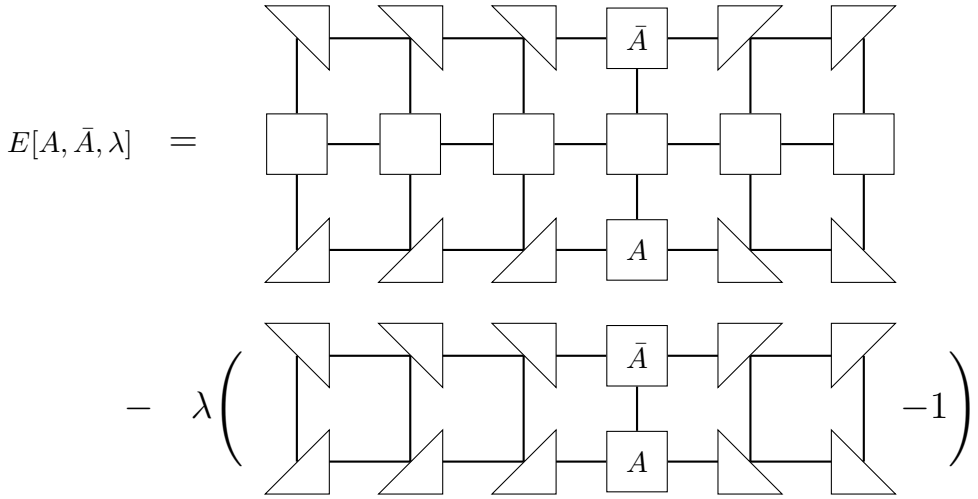


Figure 2.7: Graphic representation of Eq. (2.2.1).

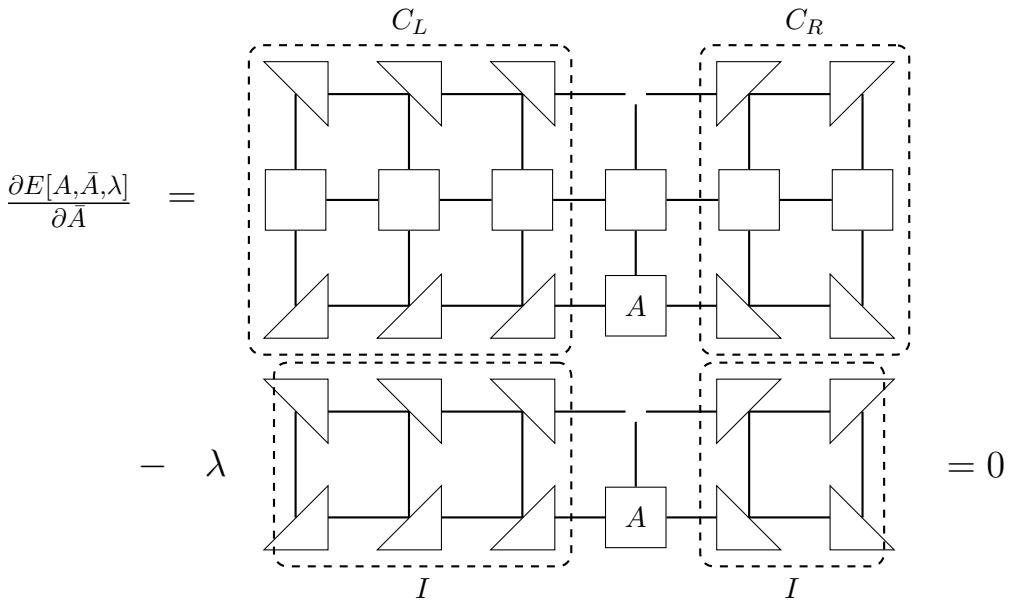


Figure 2.8: Graphic representation of Eq. (2.2.1). The derivative with respect to $\bar{A}$ is the rest of the tensor network, since the tensor contraction can be viewed as a linear function.

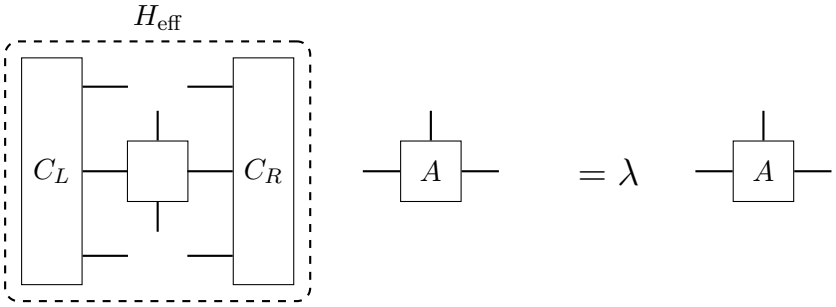


Figure 2.9: Graphic representation of Eq. (2.2.2).

Differentiating E with respect to λ gives the normalization condition, which is ensured by the mixed-canonical form of MPS.

Before moving to the next site, we need to keep the MPS in mixed-canonical form. We perform SVD to get $A_{\text{new}} = U\Sigma V^\dagger$ and keep U as the update of site i of the MPS. For the next site $i+1$, one just needs to repeat the above process.

In conclusion, the DMRG workflow is:

- Construct the MPO for the Hamiltonian H.
- Generate a random MPS and perform right-to-left SVD sweep to make it right-canonical (mixed-canonical at site 1).
- From site $i = 1$, begin the left-to-right DMRG sweep:
  - Contract tensors to obtain the environments C_L and C_R, and furthermore the effective Hamiltonian H_{eff}.
  - To save computational cost, all C_R tensors, but only the first C_L tensor, are obtained.
  - Solve $H_{\text{eff}}A = \lambda A$ to get the minimum eigenvalue $\lambda_{\min}$ and the corresponding eigenvector A_{new}.
  - Reshape A_{new} to matrix and perform SVD, keep U and reshape to tensor as the update of site i.
  - Move to site $i+1$, use the updated MPS to update C_L and get H_{eff}.
  - Repeat until site $N-1$ is updated.
- After the left-to-right sweep, all tensors are left-canonical except for site N. Thus it is better to start the sweep from the right side. Also, the C_L obtained from the left-to-right sweep can be reused.
- From site $i = N$, begin the right-to-left DMRG sweep:
  - Use the C_L from the left-to-right sweep, and contract tensors to obtain the effective Hamiltonian H_{eff}.
  - Solve $H_{\text{eff}}A = \lambda A$ to get the minimum eigenvalue $\lambda_{\min}$ and the corresponding eigenvector A_{new}.

  - Reshape A_{new} to matrix and perform SVD, keep $V^\dagger$ and reshape to tensor as the update of site i.
  - Move to site $i-1$, use the updated MPS to update C_R and get H_{eff}.
  - Repeat until site 2 is updated.

- Repeat the left-to-right and right-to-left DMRG sweeps until the variational energy $\lambda_{\min}$ is converged.

- The final MPS and $\lambda_{\min}$ are the ground-state MPS and ground-state energy, respectively.

The above workflow gives the steps of the one-site DMRG. In practice, two-site DMRG is often used. The two-site DMRG differs from the one-site DMRG when updating one site by solving the eigenvalue problem on two sites (site i and $i+1$) instead of one site (site i). Two-site DMRG requires higher computational cost, but has a better chance to escape local minima, and the truncation error $e_{\text{trunc}} = \sum_{D+1}^{dD} \sigma_j^2$ can be computed to quantify convergence. The results in Chapter 4 and Chapter 5 are obtained by two-site DMRG.

Chapter 3

Quantum phase transitions

This chapter briefly introduces quantum phase transitions (QPTs), with a focus on some key concepts that will be utilized later in this thesis. The introduction to QPTs follows the book *Quantum Phase Transitions* by Subir Sachdev [2].

QPTs occur at zero temperature, where there are no thermal fluctuations and systems stay in their ground states. The different phases are controlled by a nonthermal dimensionless parameter g, and at the critical point g_c the ground-state energy is nonanalytic and the phase transition happens [2]. g is called the control parameter of the system. Consider a system whose Hamiltonian is $H(g) = H_0 + gH_1$. For a system in a finite lattice, the ground-state energy will generally be an analytic function of g, with the exception when $[H_0, H_1] = 0$. Since H_0 and H_1 commute, they can be simultaneously diagonalized and a common set of eigenbasis $\{|\psi_i\rangle\}_{i=0}$ can be found; therefore the eigenvectors of $H(g)$ are independent of g. The energy of each level is $\langle\psi_i| H_0 + gH_1 |\psi_i\rangle = a_i + gb_i$, which means they are linear functions of g and a level crossing can happen. For example, consider a case when $a_0 < a_1$ and $b_0 > b_1$; then $E_0(g)$ and $E_1(g)$ can cross at some point g_c, leading to $E_1(g)$ becoming the new ground-state energy when $g > g_c$, and the ground-state energy is not analytic at $g = g_c$. More generally, when $[H_0, H_1] \neq 0$, there can be an avoided level crossing, meaning that there is an energy gap between the ground state and the excited state. The energy gap vanishes as lattice size grows, creating a nonanalyticity at $g = g_c$ in the infinite lattice limit. In the case of an actual level crossing, it is said to be a first-order phase transition; and in the limiting case of an avoided level crossing, it is said to be a second-order or continuous phase transition [2]. We will focus on continuous phase transitions in this thesis.

3.1 Critical exponents

The behavior of a system in the vicinity of the critical point is characterized by critical exponents, which are associated with some observables. Let the deviation from the critical point $r = (g - g_c)/g_c$ be the reduced control parameter, and assume for $r < 0$ the system is in the ordered (low-symmetry) phase and for $r > 0$ it is in the disordered (high-symmetry) phase without loss of generality.

The characteristic energy scale Δ is the characteristic energy scale of fluctuations above the ground state, and vanishes as

$$\Delta \sim |r|^{z\nu}, \tag{3.1.1}$$

where z is the dynamical critical exponent and $z\nu$ is a critical exponent. For example, Δ can be the energy gap between the lowest excitation and the ground state. For both $r < 0$ and $r > 0$ the system has the same exponent $z\nu$, but the constants of proportionality can be different [2].

Continuous quantum phase transitions have a characteristic length scale ξ, which diverges as

$$\xi \sim |r|^{-\nu}, \tag{3.1.2}$$

where ν is a critical exponent. The characteristic length could be the length scale which determines the exponential decay of correlation functions in the ground state, or the length scale at which some characteristic crossover happens and the system exhibits long-distance correlations [2]. For example, when close to the critical point, the correlation function $C(l)$ follows the power-law decay

$$C(l) \sim \frac{1}{l^{d-2+\eta}}$$

when $l \ll \xi$, and it follows the exponential decay

$$C(l) \sim e^{-l/\xi}$$

when $l \gg \xi$. Combining Eq. (3.1.1) and Eq. (3.1.2) gives the following relation:

$$\Delta \sim \xi^{-z}.$$

3.2 Quantum-classical mapping

A d-dimensional quantum system at finite temperature can be mapped to a $(d+1)$-dimensional classical system. Although the mapping is not an exact equivalence, it is very useful for studying the critical properties of continuous phase transitions using this mapping [2]. The partition function Z of a quantum system can be written as

$$Z = \mathrm{tr}\Big(\mathrm{e}^{-\beta H}\Big),$$

where $\beta = 1/(k_B T)$ and H is the Hamiltonian. Let $L_\tau = \hbar\beta$. Then $\mathrm{e}^{-\beta H}$ becomes $\mathrm{e}^{-L_\tau H/\hbar}$, which can be interpreted as the evolution operator over an imaginary time length L_τ. For simplicity we set $\hbar = 1$. Next, split the total length β into many imaginary time intervals $M \cdot \Delta\tau$; then we have

$$\mathrm{e}^{-\beta H} = \left(\mathrm{e}^{-\Delta\tau H}\right)^M,$$

and the partition function becomes

$$\begin{aligned} Z &= \mathrm{tr}\left[\left(\mathrm{e}^{-\Delta\tau H}\right)^M\right] \\ &= \sum_{v_1 \in \{v\}} \langle v_1| \left(\mathrm{e}^{-\Delta\tau H}\right)^M |v_1\rangle \\ &= \sum_{v_1,\cdots,v_M \in \{v\}} \langle v_1| \mathrm{e}^{-\Delta\tau H} |v_M\rangle \langle v_M| \cdots |v_2\rangle \langle v_2| \mathrm{e}^{-\Delta\tau H} |v_1\rangle, \end{aligned}$$

where $\{v\}$ is a complete set of basis. The matrix element $\langle v_{n+1}| \mathrm{e}^{-\Delta\tau H} |v_n\rangle$ can be interpreted as the probability amplitude of the system evolving from the state $|v_n\rangle$ to the state $|v_{n+1}\rangle$ during

the time interval $\Delta\tau$. Then the expression inside the sum gives the probability amplitude of a path $v_1 \to v_2 \to \cdots \to v_M \to v_1$, and the partition function sums over all possible paths. Formally speaking, a quantum system defined on a d-dimensional space $\mathbb{R}^d$ is mapped onto a classical system on $\mathbb{R}^d \times S^1$, where S^1 is a circle with circumference L_τ. For the 1D transverse field Ising chain (TFIC) $H = -\sum_{j=1}^{N-1} \sigma_j^z \sigma_{j+1}^z - h \sum_{j=1}^{N} \sigma_j^x$, we have the following result [2]:

$$Z = C \sum_{\{s_{i,k}\}} \exp\left(K_x \sum_{i,k} s_{i,k} s_{i+1,k} + K_\tau \sum_{i,k} s_{i,k} s_{i,k+1} \right), \tag{3.2.1}$$

where $s_{i,k}$ is the classical Ising spin at spatial site i and imaginary time site k, $\{s_{i,k}\}$ is the set of all spins, C is some normalization coefficient, $K_x = \Delta\tau$ and $K_\tau = -\frac{1}{2} \ln \tanh(\Delta\tau h)$. Eq. (3.2.1) clearly shows that the 1D quantum model is mapped to a 2D classical model, with coupling K_x in the spatial dimension and K_τ in the imaginary time dimension, respectively.

3.3 Finite-size scaling

Finite-size scaling (FSS) is the approach that extracts critical properties of an infinite system given the data of finite systems. Although phase transitions occur in infinite-size systems, we often perform numerical simulations in finite-size systems, and FSS becomes a useful tool to analyze the data.

First we introduce the scaling properties of functions. If a function $f(x)$ has the property

$$f(\lambda x) = \lambda^a f(x)$$

which is true for any $\lambda > 0$, $f(x)$ is said to have scaling properties. We can further prove $f(x)$ must follow $f(x) \sim x^a$. More generally, a function is a generalized homogeneous function if $\exists a_1, \cdots, a_n \in \mathbb{R}$ and $\forall \lambda > 0$,

$$f(\lambda^{a_1} x_1, \cdots, \lambda^{a_n} x_n) = \lambda f(x_1, \cdots, x_n).$$

Widom observed that the singular part of the free energy density, which is divergent when differentiated at the critical point, is a generalized homogeneous function in the vicinity of the critical point [2]. This is called the scaling hypothesis. Let $f(t, h)$ be the singular part of the free energy density, where t is the reduced temperature and h is the external field. It follows

$$f(\lambda^a t, \lambda^b h) = \lambda f(t, h).$$

Choose λ such that $t\lambda^a = 1$, we have

$$f(t, h) = t^{\frac{1}{a}} f(1, h t^{-\frac{b}{a}}),$$

which gives rise to the data collapse approach in data analysis. Suppose we have the data (h, f) at t_1 and t_2, we can draw a curve with points $(h t_1^{-b/a}, f t_1^{-1/a})$, and another curve with points $(h t_2^{-b/a}, f t_2^{-1/a})$, and these two curves will collapse to one curve $f(1, x)$ since

$$t^{-\frac{1}{a}} f(t, h) = f(1, h t^{-\frac{b}{a}}).$$

The above demonstration is based on classical thermodynamics and infinite systems, but it can be extended to quantum phase transitions and finite systems. For an observable O, we include the system size L as a new variable in the scaling form with a scaling power of -1. Then the scaling form of O can be written as

$$O_L(r) = b^{-y_r\omega} O_{L/b}(b^{y_r} r),$$

where r is the reduced control parameter, $O(r) \sim |r|^{\omega}$, y_r is the scaling power of r and b is the scaling parameter. We can choose a reference length L_0 and scale O to L_0 by setting $b = L/L_0$,

$$O_L(r) = \left(\frac{L}{L_0}\right)^{-y_r\omega} O_{L_0}\left(\left(\frac{L}{L_0}\right)^{y_r} r\right).$$

Let $L_0 = 1$, the scaling function $\Psi_O(rL^{y_r})$ can be introduced as

$$O_L(r) = L^{-y_r\omega}\Psi_O(rL^{y_r}), \tag{3.3.1}$$

and the data collapse to the scaling function as

$$y = \Psi_O(x),$$

where $y = O_L L^{y_r\omega}$ and $x = rL^{y_r}$.

In the presence of irrelevant variables, Eq. (3.3.1) should be rewritten as

$$O_L(r, u) = L^{-x_O}\Psi(rL^{y_r}, uL^{y_u}),$$

where u is the irrelevant variable. It is useful to perform a Taylor expansion with respect to u:

$$\Psi(rL^{y_r}, uL^{y_u}) = \Psi_0(rL^{y_r}) + uL^{y_u}\Psi_1(rL^{y_r}) + \frac{u^2L^{2y_u}}{2}\Psi_2(rL^{y_r}) + \cdots.$$

The coefficients, together with u, can be absorbed into the functions Ψ_i. In general, when multiple irrelevant variables exist, we have

$$O_L(r) = L^{-x_O}\left[\Psi_0(rL^{y_r}) + L^{-\omega_1}\Psi_1(rL^{y_r}) + L^{-\omega_2}\Psi_2(rL^{y_r}) + \cdots\right].$$

For a non-zero dimensionless quantity, it neither diverges nor converges to zero; therefore $x_O = 0$. Then at the critical point $r = 0$, the above expression becomes

$$O_L(0) = O_\infty + a_1L^{-\omega_1} + a_2L^{-\omega_2} + \cdots, \tag{3.3.2}$$

where $O_\infty = \Psi_0(0)$, $a_i = \Psi_i(0)$ and ω_i are called correction exponents.

3.4 Crosscap overlaps

The crosscap overlap $\langle C|\psi\rangle$ is the overlap between a crosscap state $|C\rangle$ and a quantum state $|\psi\rangle$. The crosscap overlap is useful for studying the quantum phase transitions. The Klein bottle entropy, which has been shown to be a universal scaling function near critical points, is the modulus square of the crosscap overlap [20]. The Luttinger parameter, which controls the low-energy physics of Tomonaga-Luttinger liquids[1], can be extracted from a single wave

[1] In one dimension, interacting fermionic systems are described by the Tomonaga-Luttinger liquid.

function by computing crosscap overlaps [21]. The criticality of 2D classical Ising model and 1D quantum transverse-field Ising model can be described by the 2D Ising conformal field theory (CFT), in which two Ising crosscap states can be constructed and mapped to each other by the Kramers-Wannier duality transformation [22].

Here we focus on one of the Ising crosscap states and introduce the known results. Consider the TFIC with Hamiltonian

$$H = -\sum_{j=1}^{N} \sigma_j^z \sigma_{j+1}^z - h \sum_{j=1}^{N} \sigma_j^x.$$

The lattice crosscap state $|C_{\text{latt}}\rangle$ is the product of Bell pairs identifying Ising spins at pairs of antipodal sites [22]:

$$|C_{\text{latt}}\rangle = \prod_{j=1}^{N/2} \left(|\uparrow_j \uparrow_{j+N/2}\rangle + |\downarrow_j \downarrow_{j+N/2}\rangle \right),$$

where the lattice size N must be even. Ising spins at two antipodal sites j and $j + N/2$ are identified by maximally entangled Bell pairs, which corresponds to the crosscap boundary condition. The crosscap overlap $\langle C_{\text{latt}}|\psi_0\rangle$ is the overlap between the lattice crosscap state $|C_{\text{latt}}\rangle$ and the ground state $|\psi_0\rangle$. In the continuum limit, the TFIC at the critical point is described by the 2D Ising CFT. The following result for the crosscap overlap can be obtained by conformal perturbation theory [22]:

$$\langle C|\psi_0(s)\rangle = \sqrt{\frac{2+\sqrt{2}}{2}} + \sqrt{\frac{2-\sqrt{2}}{2}} \frac{\pi}{4} \cdot s - \sqrt{\frac{2+\sqrt{2}}{2}} \frac{\pi^2}{32} \cdot s^2 + \mathcal{O}(s^3), \tag{3.4.1}$$

where $s = (h - h_c)L$ and L is the length of the TFIC. Eq. (3.4.1) shows that at the critical point, the crosscap overlap has an exact value $\sqrt{\frac{2+\sqrt{2}}{2}}$ independent of the system size. This makes the crosscap overlap an ideal indicator for pinpointing the critical point of the TFIC.

Numerically, the crosscap overlap can be extracted from the ground-state MPS by contracting the tensors at antipodal sites [21], as shown in Fig. 3.1.

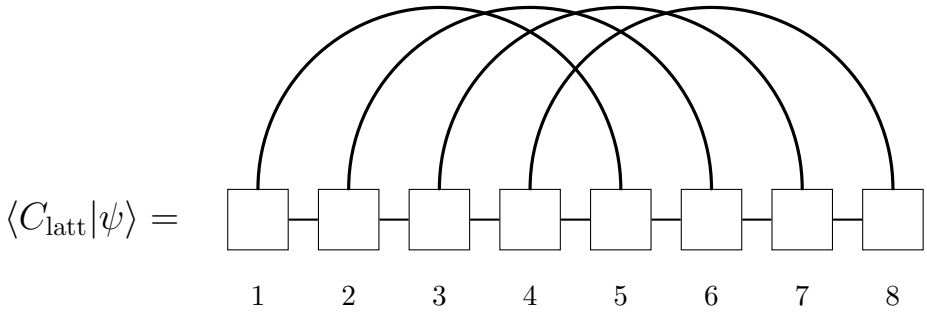


Figure 3.1: Extracting crosscap overlap from ground-state MPS [21]. Tensors at site i and site $i + N/2$ are contracted. This figure shows the case when $N = 8$.

Chapter 4

Some exactly solvable models and their DMRG results

In this chapter, we test our DMRG code on some exactly solvable spin-1/2 chains and the results obtained from DMRG are compared to the exact values. The DMRG code was implemented from scratch by the author and is openly available from the Github repository.

4.1 The Heisenberg chain

The Heisenberg chain has the Hamiltonian

$$H = \sum_{i=1}^{N} S_i^x S_{i+1}^x + S_i^y S_{i+1}^y + S_i^z S_{i+1}^z,$$

where $S_{N+1}^{\alpha} = S_1^{\alpha}$ $(\alpha = x, y, z)$ under periodic boundary conditions. Fig. 4.1 shows the relative errors between DMRG ground-state energies and the exact values obtained by numerically solving the Bethe ansatz[1] equations. The relative error of a quantity A is defined as $(A_{\text{estimate}} - A_{\text{true}})/A_{\text{true}}$ in this thesis.

4.2 The XXZ chain

The spin-1/2 XXZ chain has the Hamiltonian

$$H = \sum_{i=1}^{N} S_i^x S_{i+1}^x + S_i^y S_{i+1}^y + \Delta S_i^z S_{i+1}^z,$$

where Δ is a tuning parameter. The Luttinger parameter K has an exact value $\pi/[2(\pi - \arccos\Delta)]$. K can also be obtained by $|\langle C|\psi_0\rangle|^2 = \frac{1}{\sqrt{K}}$ [21], where $|\langle C|\psi_0\rangle|$ is the crosscap overlap, which can be extracted from the ground-state MPS. Fig. 4.2 shows the DMRG results along with the exact values.

[1] Bethe ansatz is used to exactly solve the 1D integrable quantum many-body systems.

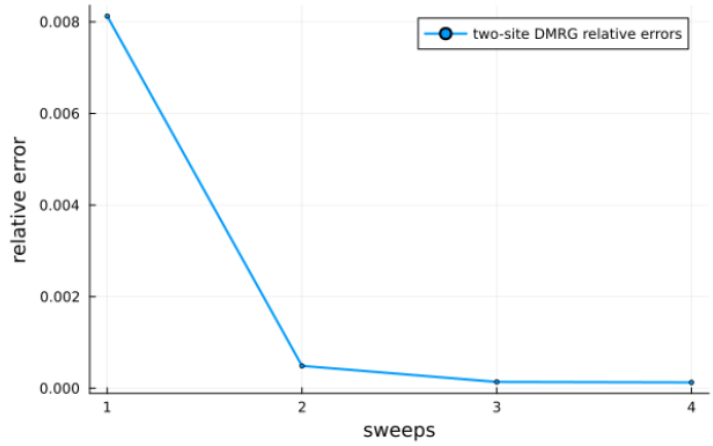


Figure 4.1: Relative errors of the ground-state energy of a spin-1/2 Heisenberg chain with $N = 50$ sites and periodic boundary conditions. A random MPS with bond dimension $D = 50$ is chosen to be the initial MPS.

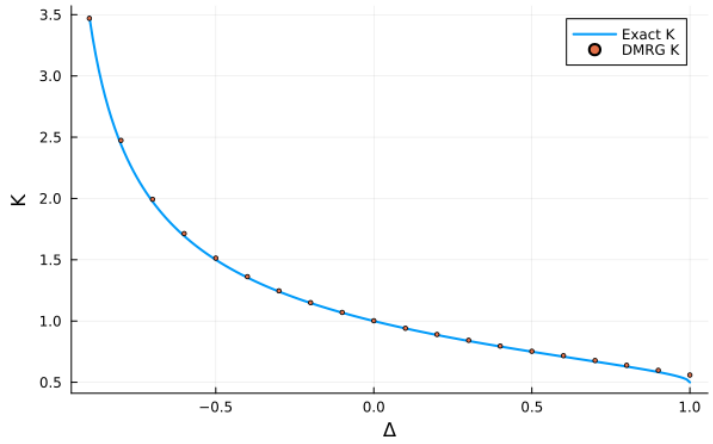


Figure 4.2: Luttinger parameter K extracted from the ground-state MPS of 20-site XXZ chain compared with exact values. A random MPS with bond dimension $D = 30$ is chosen to be the initial MPS. At $\Delta = 1$, there is a clear deviation, which is due to a marginally irrelevant operator causing strong finite-size effects[21].

4.3 The Haldane-Shastry model

The spin-1/2 Haldane-Shastry model has the Hamiltonian [21]

$$H = \left(\frac{\pi}{N}\right)^2 \sum_{1\le i<j\le N} \frac{\vec{S}_i \cdot \vec{S}_j}{\sin^2[\frac{\pi}{N}(i-j)]},$$

where $\vec{S} = (S^x, S^y, S^z)$. The crosscap overlaps have the exact values

$$|\langle C|\psi_0\rangle|^2 = \frac{2^M (M!)^3}{[(M/2)!]^2 (2M)!},$$

where $M = N/2$ and $\mathrm{mod}(N, 4) = 0$ [22]. Fig. 4.3 shows the crosscap overlaps extracted from the ground-state MPS and the exact values.

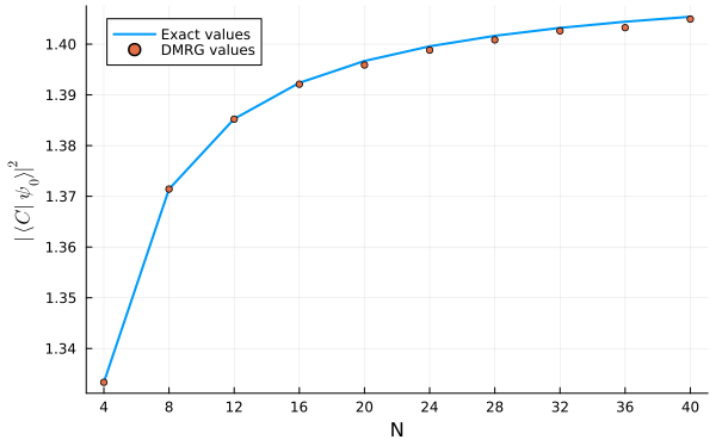


Figure 4.3: Crosscap overlaps of N-site Haldane-Shastry model for $N = 4, 8, \cdots, 40$.

4.4 The transverse-field Ising chain

The transverse-field Ising chain has the Hamiltonian

$$H = -\sum_{j=1}^{N} \sigma_j^x \sigma_{j+1}^x - h \sum_{j=1}^{N} \sigma_j^z.$$

As discussed in Section 3.4, the crosscap overlap has an exact value $\sqrt{\frac{2+\sqrt{2}}{2}}$ independent of the system size at the critical point. The crosscap overlaps obtained by the DMRG algorithm for different values of N and h are shown in Fig. 4.4, which clearly indicates the critical point. In the vicinity of the critical point $h_c = 1$, data collapse is applied as a verification. The curves for different sizes clearly collapse on the same curve, as shown in Fig. 4.5.

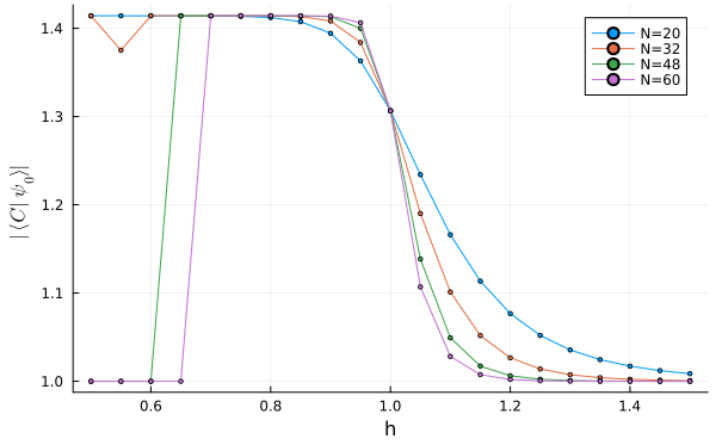


Figure 4.4: Crosscap overlaps of N-site TFIC for $N = 20, 32, 48, 60$ at different values of the external field h, with $h = 0.5, 0.55, 0.6, \cdots, 1.5$. For $0 < h < 1$, the actual ground state is the superposition state $|z_0\rangle + |z_1\rangle$, where $|z_i\rangle$ are the two $\mathbb{Z}_2$-symmetry-breaking states. At some points ($N = 48$, $h \leq 0.6$; $N = 60$, $h \leq 0.65$) the DMRG algorithm converges to one of the $\mathbb{Z}_2$-symmetry-breaking states instead of the actual ground state. At the point ($N = 32$, $h = 0.55$) the DMRG algorithm does not fully converge, likely due to reaching the maximum sweep limit.

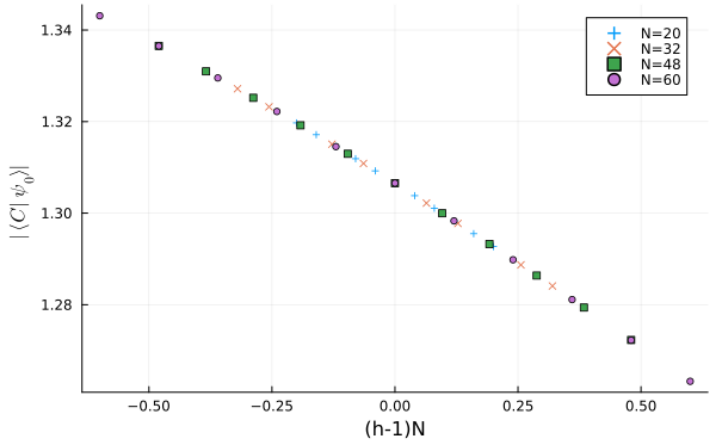


Figure 4.5: Data collapse of the TFIC in the vicinity of the critical point $h_c = 1$.

Chapter 5

The long-range transverse-field Ising chain (LRTFIC)

The long-range transverse-field Ising chain (LRTFIC) has the Hamiltonian

$$H = -\sum_{1\leq i<j\leq N} J_{ij}\sigma_i^z\sigma_j^z - h\sum_{i=1}^{N}\sigma_i^x,$$

where h is the external transverse field. The coupling strength

$$J_{ij} = \frac{J}{|\frac{N}{\pi}\sin\left[\frac{\pi}{N}(i-j)\right]|^\alpha}$$

describes the chain evenly placed on a circular lattice with circumference N. The chord distance between site i and site j is $|\frac{N}{\pi}\sin\left[\frac{\pi}{N}(i-j)\right]|$, which means J_{ij} decays as a power law with respect to distance with a decay exponent α. For $J > 0$ the coupling is ferromagnetic and for $J < 0$ the coupling is antiferromagnetic. In this chapter we focus only on the ferromagnetic case and set $J = 1$ without loss of generality. Similar to the TFIC, the non-commutativity between the Ising interaction term and the transverse-field term causes quantum fluctuations, which can give rise to a quantum phase transition between the ordered phase (small h) and the disordered phase (large h).

In this chapter, we first briefly review the previous studies of the LRTFIC and summarize the important properties of the LRTFIC. Next, we will demonstrate the process of pinpointing the critical point of the LRTFIC for $\alpha = 3.5$, using the DMRG algorithm and the crosscap overlaps. Finally, the results for the LRTFIC will be presented.

5.1 Previous studies on the LRTFIC

5.1.1 Limiting cases of the LRTFIC

First we consider the limiting cases when the field $h \to \infty$ and $h \to 0$, as well as the decay exponent $\alpha \to \infty$ and $\alpha \to 0$. The following results are based on the TFIC, but apply to LRTFIC since studies show that the LRTFIC shows a quantum phase transition between a field-polarized phase and a spin-aligned phase for all values of α [27].

$h \to \infty$:

For a large field h, the ground state is the x-polarized state:

$$|\psi_0\rangle = \prod_i |{\to}\rangle_i \,,$$

where $|{\to}\rangle$ is the eigenstate of σ^x with $\sigma_i^x \,|{\to}\rangle_i = |{\to}\rangle_i$.

$h \to 0$:

If $h = 0$ exactly, the ground state is two-fold degenerate:

$$|{\Uparrow}\rangle = \prod_i |{\uparrow}\rangle_i \,, \quad |{\Downarrow}\rangle = \prod_i |{\downarrow}\rangle_i \,, \tag{5.1.1}$$

and any superposition of these two states can be the ground state. For small $h > 0$, the degeneracy is broken and a doublet with a small splitting remains [2]

$$|\psi_+\rangle = \frac{|{\Uparrow}\rangle + |{\Downarrow}\rangle}{\sqrt{2}}, \quad |\psi_-\rangle = \frac{|{\Uparrow}\rangle - |{\Downarrow}\rangle}{\sqrt{2}},$$

where $|\psi_+\rangle$ is the ground state and $|\psi_-\rangle$ is the lowest excited state [28]. The splitting $\Delta E = E_- - E_+$ vanishes as the system size grows, and Eq. (5.1.1) again becomes the ground state in the thermodynamic limit. Physically, symmetry breaking happens and the system will choose to be the all-up or all-down state instead of a random superposition state.

$\alpha \to \infty$ or $\alpha \to 0$:

For a large α, the coupling J_{ij} decays quickly and the system behaves like a short-range model. For a small α, the long-range coupling becomes significant and the system belongs to a different universality class than the TFIC.

5.1.2 Critical regimes of the LRTFIC

The LRTFIC belongs to different regimes depending on the decay exponent α. Using the common notation, we set $\alpha = d + \sigma$, where d is the spatial dimension and $d = 1$ for a chain. It was first proved that for $\sigma > 2$ the LRTFIC belongs to the short-range regime by mean-field theory [9]. The exact boundary for the short-range regime was calculated to be $\sigma_* = 2 - \eta_{SR} = 7/4$ by renormalization group, where $\eta_{SR} = 1/4$ is the anomalous dimension of the chain when $\sigma = 2$ [10]. For $\sigma \leq 2/3$, the quantum phase transitions are described by the mean-field theory [27]. For $2/3 < \sigma < 7/4$, the critical exponents vary continuously with σ and connect the long-range mean-field regime and the short-range regime. The boundary $\sigma_* = 7/4$ has been further verified numerically by quantum Monte Carlo methods [16]. The phase diagram is summarized in Fig. 5.1.

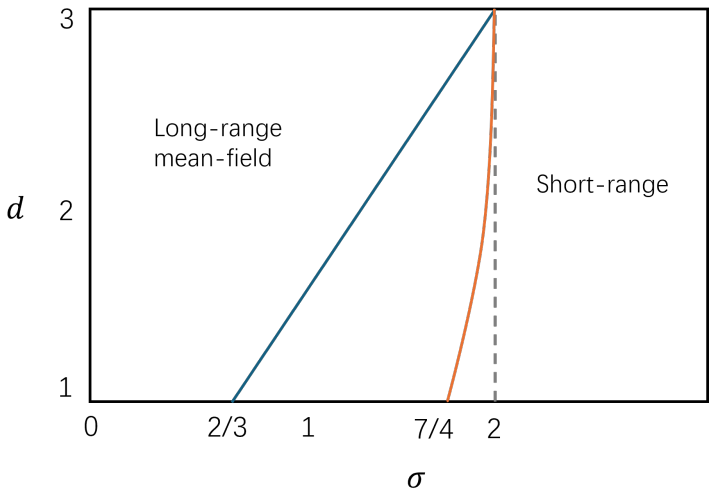


Figure 5.1: Phase diagram of LRTFIM. The y-axis label d denotes the dimension. The orange solid curve is the boundary given by renormalization group and the gray dotted line is the boundary given by mean-field theory. The blue solid line is the boundary of the long-range mean-field regime. Here long-range mean-field is the name for this regime, meaning it belongs to the long-range regime and can be described by the mean-field theory.

5.2 DMRG results on the LRTFIC

For the LRTFIC, it belongs to the short-range TFIC universality when $\alpha > 11/4$. Therefore, the crosscap overlap at the critical point are expected to have the same exact value, as discussed in Section 3.4.

In this section, we will take $\alpha = 3.5$ as an example to demonstrate the process of pinpointing the critical point of the LRTFIC. First, we run the DMRG algorithm on systems with sizes $N = 32, 48, 60, 80$ over a large range of h and obtain their ground-state MPS. Next, we extract the crosscap overlap values based on Fig. 3.1 and plot them to estimate the critical point h_c, as shown in Fig. 5.2. The crosscap overlap values cross at $h \approx 1.24$, but the value at $h = 1.24$ clearly deviates from the exact value. The reason is that finite-size effects are large and the systems are too small. To get a more precise estimate, the DMRG algorithm is run on $N = 240, 280$ and the results are shown in Fig. 5.3. Now the new estimated h_c becomes 1.249 and the crosscap overlap value at this point approaches the exact value more closely, with a relative error $\approx 1.6\%$. Then, according to the finite-size scaling Eq. (3.3.2), the crosscap overlaps should follow a power-law decay as system size grows. Therefore we try to fit the data points of different N at some certain h to the following function:

$$\langle C|\psi_0\rangle_N = \langle C|\psi_0\rangle_\infty + a_1 N^{-\omega_1} + a_2 N^{-\omega_2},$$

where $\langle C|\psi_0\rangle_N$ is the crosscap overlap for finite size N, and $\langle C|\psi_0\rangle_\infty$, a_1, a_2, ω_2 are parameters to be fitted. Here ω_1 is set to $\alpha - \alpha_* = 0.75$ which represents the correction exponent for the long-range interaction [11], and ω_2 represents the subleading exponent or the effective exponent for all other exponents.

In Fig. 5.3, we can see that $\langle C|\psi_0\rangle_{N=240}$ is smaller than $\langle C|\psi_0\rangle_{N=280}$ at $h = 1.249$. Therefore, the search for the critical point is started from $h = 1.250$, with a step size $\Delta h = 0.001$.

If at some h, the fitted value $\langle C|\psi_0\rangle_\infty$ is close to the exact value $\sqrt{\frac{2+\sqrt{2}}{2}} \approx 1.3066$, we can conclude that this h is the critical point. Fig. 5.4 shows the fitted curve at $h = 1.25$. The fitted value $\langle C|\psi_0\rangle_\infty \approx 1.3064$ has a relative error 0.02%. The estimated critical point $h_c = 1.25$ is consistent with previous studies [15, 16]. Finally, the data collapse is shown in Fig. 5.5 as a further verification.

Following the above process, we determine the critical points for $\alpha = 3, 3.5, 4$. The results are listed in Table 5.1.

Table 5.1: Critical points h_c of the LRTFIC for different α.

α	3.0	3.5	4.0
h_c	1.421	1.250	1.156

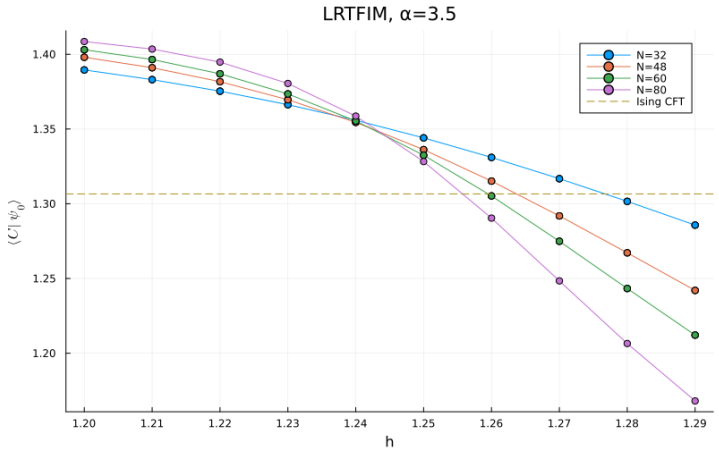


Figure 5.2: Crosscap overlap values extracted from ground-state MPS obtained by the DMRG algorithm for $N = 32, 48, 60, 80$.

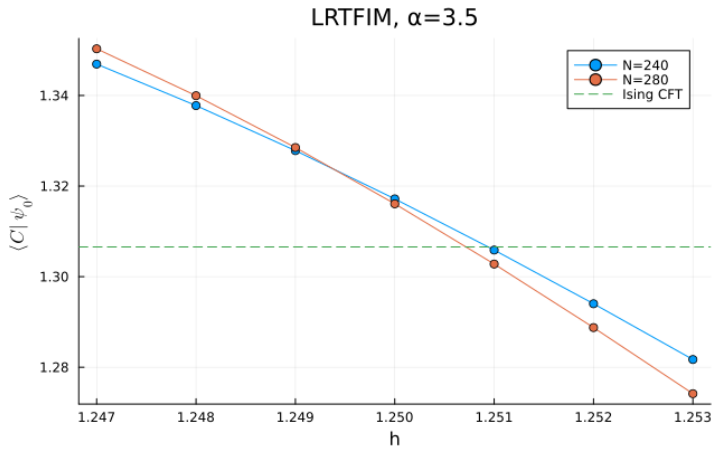


Figure 5.3: Crosscap overlap values extracted from ground-state MPS obtained by the DMRG algorithm for $N = 240, 280$.

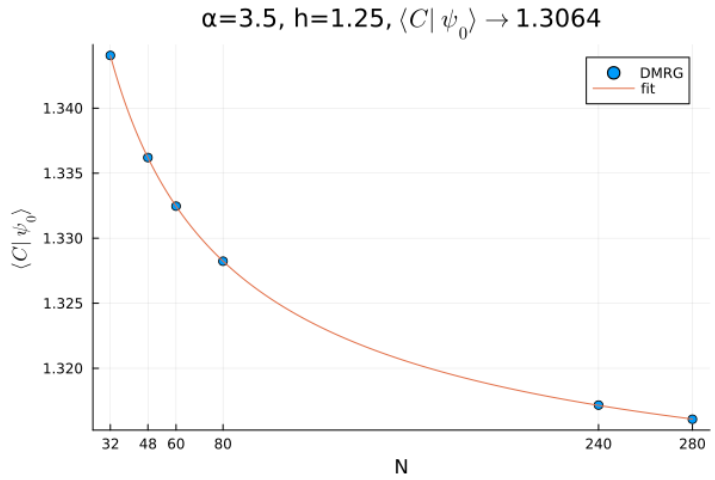


Figure 5.4: Crosscap overlap values at $h = 1.25$ are fitted to a power-law decay curve. The fitted value is $\langle C|\psi_0\rangle_\infty \approx 1.3064$. The fitting is also performed on $h = 1.251$ and $h = 1.252$, and their fitted values of $\langle C|\psi_0\rangle_\infty$ have larger deviations than the $h = 1.25$ case.

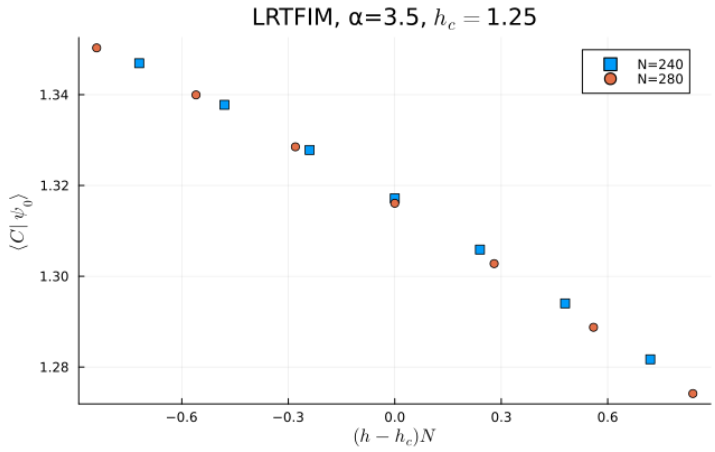


Figure 5.5: Data collapse of crosscap overlap values in the vicinity of $h = 1.25$.

Chapter 6

Summary and outlook

In this thesis, we studied the critical behavior of the ferromagnetic long-range transverse-field Ising chain (LRTFIC) using the density matrix renormalization group (DMRG). The main goal was to test whether the crosscap overlap, which is known to provide a clean indicator of the critical point in the short-range transverse-field Ising chain (TFIC), can also be used to locate critical points in the LRTFIC.

We first reviewed the tensor-network language and the DMRG algorithm, including matrix product states, matrix product operators, canonical forms of MPS, and the one-site DMRG algorithm that optimizes MPS variationally. Also, the entanglement area law was emphasized as the key reason why the MPS can use a fixed bond dimension. We then introduced several concepts related to quantum phase transitions, such as critical exponents, quantum-classical mapping, finite-size scaling and the crosscap overlap. These concepts provide the theoretical background for interpreting numerical data obtained from finite systems.

Before applying the method to the LRTFIC, we tested the DMRG implementation on several exactly solvable spin-1/2 chains. The two-site DMRG algorithm was used in practice to achieve better convergence. For the Heisenberg chain, the ground-state energy obtained from DMRG was compared with the exact result from the Bethe ansatz. For the TFIC, the crosscap overlap extracted from the ground-state MPS was shown to identify the critical point accurately, and the data collapse near the critical point further confirmed the expected scaling behavior. The XXZ chain and the Haldane-Shastry model were also used as benchmark examples for extracting quantities that are related to crosscap overlaps from DMRG ground states.

The numerical results presented in this thesis provide estimates of the critical points of the LRTFIC. For $\alpha = 3.5$, the crosscap overlap curves for different system sizes first gave an estimate of the critical point near $h_c \approx 1.24$. However, the crosscap overlap value at this crossing still showed visible finite-size corrections. By including larger system sizes up to $N = 280$ and fitting the finite-size corrections, we obtained the estimate $h_c \approx 1.25$. At this value, the extrapolated crosscap overlap is very close to the exact short-range Ising value. Applying the same procedure to other decay exponents gave critical points for $\alpha = 3$, 3.5, and 4, all consistent with previous numerical studies.

These results suggest that the crosscap overlap can serve as a useful numerical probe of criticality in long-range interacting spin chains, when the system belongs to the short-range Ising universality class. Compared with more traditional quantities such as magnetization, susceptibility, or Binder cumulants, the crosscap overlap provides a direct connection to universal

properties of the underlying conformal field theory. This makes it a complementary observable for studying quantum critical points with tensor-network methods.

There are several directions for future work. First, this thesis mainly focuses on the ferromagnetic Ising coupling with decay exponents in the short-range regime. It would be interesting to investigate smaller values of α, especially in the intermediate regime where the critical exponents vary continuously with α. In that regime, the critical theory is no longer the short-range Ising CFT, and the behavior of the crosscap overlap may contain new universal information. Another interesting direction is to extend the study to the antiferromagnetic case, whose critical behavior is less understood then the ferromagnetic case. Exploring the crosscap overlap in these systems may provide new insights into their criticality.

Second, the finite-size corrections in the LRTFIC are significant. A more systematic study with larger system sizes, larger bond dimensions, and more careful convergence analysis would help improve the precision of the estimated critical points. It would also be useful to compare different fitting forms for the finite-size corrections, especially when several irrelevant exponents may contribute at the same time.

Finally, the crosscap overlap can be studied in other long-range quantum spin models and in models with different universality classes. Such studies could clarify how broadly the crosscap overlap can be used as numerical probes of criticality, and whether it can reveal universal data that are difficult to extract from conventional observables.

Bibliography

[1] P. Pfeuty, "The one-dimensional ising model with a transverse field," *ANNALS of Physics*, vol. 57, no. 1, pp. 79–90, 1970.

[2] S. Sachdev, *Quantum Phase Transitions*. Cambridge University Press, 2011.

[3] R. Coldea, D. Tennant, E. Wheeler, E. Wawrzynska, D. Prabhakaran, M. Telling, K. Habicht, P. Smeibidl, and K. Kiefer, "Quantum criticality in an ising chain: experimental evidence for emergent e8 symmetry," *Science*, vol. 327, no. 5962, pp. 177–180, 2010.

[4] R. Islam, E. Edwards, K. Kim, S. Korenblit, C. Noh, H. Carmichael, G.-D. Lin, L.-M. Duan, C.-C. Joseph Wang, J. Freericks *et al.*, "Onset of a quantum phase transition with a trapped ion quantum simulator," *Nature communications*, vol. 2, no. 1, p. 377, 2011.

[5] P. Schauß, M. Cheneau, M. Endres, T. Fukuhara, S. Hild, A. Omran, T. Pohl, C. Gross, S. Kuhr, and I. Bloch, "Observation of spatially ordered structures in a two-dimensional rydberg gas," *Nature*, vol. 491, no. 7422, pp. 87–91, 2012.

[6] A. Friedenauer, H. Schmitz, J. T. Glueckert, D. Porras, and T. Schätz, "Simulating a quantum magnet with trapped ions," *Nature Physics*, vol. 4, no. 10, pp. 757–761, 2008.

[7] C. Castelnovo, R. Moessner, and S. L. Sondhi, "Magnetic monopoles in spin ice," *Nature*, vol. 451, no. 7174, pp. 42–45, 2008.

[8] P. Chakraborty, P. Henelius, H. Kjønsberg, A. Sandvik, and S. Girvin, "Theory of the magnetic phase diagram of li ho f 4," *Physical Review B—Condensed Matter and Materials Physics*, vol. 70, no. 14, p. 144411, 2004.

[9] M. E. Fisher, S.-k. Ma, and B. Nickel, "Critical exponents for long-range interactions," *Physical Review Letters*, vol. 29, no. 14, p. 917, 1972.

[10] J. Sak, "Recursion relations and fixed points for ferromagnets with long-range interactions," *Physical Review B*, vol. 8, no. 1, p. 281, 1973.

[11] N. Defenu, A. Trombettoni, and S. Ruffo, "Criticality and phase diagram of quantum long-range o (n) models," *Physical Review B*, vol. 96, no. 10, p. 104432, 2017.

[12] C. Monroe, W. C. Campbell, L.-M. Duan, Z.-X. Gong, A. V. Gorshkov, P. W. Hess, R. Islam, K. Kim, N. M. Linke, G. Pagano *et al.*, "Programmable quantum simulations of spin systems with trapped ions," *Reviews of Modern Physics*, vol. 93, no. 2, p. 025001, 2021.

[13] A. W. Sandvik, "Stochastic series expansion method for quantum ising models with arbitrary interactions," *Physical Review E*, vol. 68, no. 5, p. 056701, 2003.

[14] S. Humeniuk, "Quantum monte carlo study of long-range transverse-field ising models on the triangular lattice," *Physical Review B*, vol. 93, no. 10, p. 104412, 2016.

[15] J. A. Koziol, A. Langheld, S. C. Kapfer, and K. P. Schmidt, "Quantum-critical properties of the long-range transverse-field ising model from quantum monte carlo simulations," *Physical Review B*, vol. 103, no. 24, p. 245135, 2021.

[16] S. Shiratani and S. Todo, "Stochastic parameter optimization analysis of dynamical quantum critical phenomena in the long-range transverse-field ising chain," *Physical Review E*, vol. 110, no. 6, p. 064106, 2024.

[17] D. Vodola, L. Lepori, E. Ercolessi, and G. Pupillo, "Long-range ising and kitaev models: phases, correlations and edge modes," *New Journal of Physics*, vol. 18, no. 1, p. 015001, 2016.

[18] G. Sun, "Fidelity susceptibility study of quantum long-range antiferromagnetic ising chain," *Physical Review A*, vol. 96, no. 4, p. 043621, 2017.

[19] S. Saadatmand, S. Bartlett, and I. McCulloch, "Phase diagram of the quantum ising model with long-range interactions on an infinite-cylinder triangular lattice," *Physical Review B*, vol. 97, no. 15, p. 155116, 2018.

[20] Y. Zhang, A. Hulsch, H.-C. Zhang, W. Tang, L. Wang, and H.-H. Tu, "Universal scaling of klein bottle entropy near conformal critical points," *Physical Review Letters*, vol. 130, no. 15, p. 151602, 2023.

[21] B.-Y. Tan, Y. Zhang, H.-C. Zhang, W. Tang, L. Wang, H.-H. Tu, and Y.-H. Wu, "Extracting the luttinger parameter from a single wave function," *Physical Review Letters*, vol. 134, no. 7, p. 076501, 2025.

[22] Y. Zhang, Y.-H. Wu, L. Wang, and H.-H. Tu, "Crosscap states and duality of ising field theory in two dimensions," *Physical Review B*, vol. 113, no. 6, p. L060412, 2026.

[23] M. Fannes, B. Nachtergaele, and R. F. Werner, "Finitely correlated states on quantum spin chains," *Communications in mathematical physics*, vol. 144, no. 3, pp. 443–490, 1992.

[24] M. B. Hastings, "An area law for one-dimensional quantum systems," *Journal of statistical mechanics: theory and experiment*, vol. 2007, no. 08, pp. P08 024–P08 024, 2007.

[25] P. Calabrese and J. Cardy, "Entanglement entropy and quantum field theory," *Journal of statistical mechanics: theory and experiment*, vol. 2004, no. 06, p. P06002, 2004.

[26] G. M. Crosswhite and D. Bacon, "Finite automata for caching in matrix product algorithms," *Physical Review A—Atomic, Molecular, and Optical Physics*, vol. 78, no. 1, p. 012356, 2008.

[27] A. Dutta and J. Bhattacharjee, "Phase transitions in the quantum ising and rotor models with a long-range interaction," *Physical Review B*, vol. 64, no. 18, p. 184106, 2001.

[28] R. Shankar, *Quantum Field Theory and Condensed Matter*. Cambridge University Press, 2017.

Master's Theses in Mathematical Sciences 2026:E90
ISSN 1404-6342

LUNFBV-3021-2026

Computational Science
Centre for Mathematical Sciences
Lund University
Box 118, SE-221 00 Lund, Sweden

http://www.maths.lu.se/